Biomaterials 34 (2013) 4078–4088

Contents lists available at SciVerse ScienceDirect

Biomaterials

journal homepage: www.elsevier.com/locate/biomaterials

Near-infrared laser light mediated cancer therapy by photothermal effect of Fe_3O_4 magnetic nanoparticles

Maoquan Chu [a,*], Yuxiang Shao [a], Jinliang Peng [b], Xiangyun Dai [a], Haikuo Li [c], Qingsheng Wu [d], Donglu Shi [e]

[a] School of Life Science and Technology, Tongji University, Shanghai 200092, PR China
[b] Med-X Institute of Shanghai Jiaotong University, Shanghai 200240, PR China
[c] Shanghai Institute of Applied Physics, Chinese Academy of Sciences, Shanghai 201800, PR China
[d] Department of Chemistry, Tongji University, Shanghai 200092, PR China
[e] The Institute for Advanced Materials & Nano Biomedicine, Tongji University, Shanghai 200092, PR China

ARTICLE INFO

Article history:
Received 31 December 2012
Accepted 28 January 2013
Available online 5 March 2013

Keywords:
Fe_3O_4 nanoparticles
Near-infrared laser
Cancer
Photothermal therapy

ABSTRACT

The photothermal effect of Fe_3O_4 magnetic nanoparticles is investigated for cancer therapy both in vitro and in vivo experiments. Heat is found to be rapidly generated by red and near-infrared (NIR) range laser irradiation of Fe_3O_4 nanoparticles with spherical, hexagonal and wire-like shapes. These Fe_3O_4 nanoparticles are coated with carboxyl-terminated poly (ethylene glycol)-phospholipid for enhanced dispersion in water. The surface-functionalized Fe_3O_4 nanoparticles can be taken up by esophageal cancer cells and do not obviously affect the cell structure and viability. Upon irradiation at 808 nm however, the esophageal cancer cell viability is effectively suppressed, and the cellular organelles are obviously damaged when incubated with the NIR laser activated Fe_3O_4 nanoparticles. Mouse esophageal tumor growth was found to be significantly inhibited by the photothermal effect of Fe_3O_4 nanoparticles, resulting in effective tumor reduction. A morphological examination revealed that after a photothermal therapy, the tumor tissue structure exhibited discontinuation, the cells were significantly shriveled and some cells have finally disintegrated.

1. Introduction

Superparamagnetic iron oxide nanoparticles have been widely used in biomedical research for their unique magnetic properties, non-toxicity, and biocompatibility. Research on superparamagnetic nanoparticles has been extensively carried out on drug delivery, medical imaging, cell targeting, and hyperthermia therapy [1–8]. Cancer hyperthermal treatment [5–8] using superparamagnetic nanoparticles is of particular interest as they pose much less side effects compared with chemotherapy or radiotherapy [9]. Magnetic hyperthermia of iron oxide nanoparticles is caused via dipole relaxation induced by an alternating magnetic field (AMF) [10]. The heat generated by the locally injected magnetic nanoparticles can specifically destroy tumors, but pose minimal damage to healthy tissues. The local temperature can also be easily controlled by the AMF power and nanoparticle concentrations in the tumor. Although magnetic hyperthermia has been clinically used [5–8], the technique requires high current and voltage due to large air volume within the applied field in which energy cannot be easily focused. The photothermal effect of Fe_3O_4/alumina [11]and Fe_3O_4/mSiO_2 [12] core–shell nanoparticles for killing bacteria and KB cancer cells have been recently reported. However, how the photothermal effect of the magnetic Fe_3O_4 nanoparticles is influencing the cell and tumor tissue structures is not clear. In this study, the photothermal effect was investigated for cancer therapy with Fe_3O_4 nanoparticles of various shapes, while red and near-infrared (NIR) laser light irradiations were used to induce the photothermal effect in vitro and in vivo. A cancer cell being killed by the photothermal effect of Fe_3O_4 nanoparticles is schematically shown in Fig. 1.

With the efficient photothermal effect of magnetic Fe_3O_4 nanoparticles, it may be possible to clinically apply a hyperthermia cancer therapy using NIR instead of AMF and a human esophageal cancer model was used for the treatment. Esophageal cancer is common worldwide, but with a particularly high prevalence in China [13]. More than half of the esophageal cancer cases are diagnosed at an advanced incurable stage and many patients decline from surgical resection. For patients with inoperable esophageal cancer, local treatments such as laser-induced photodynamic therapy [14,15], hyperthermia [15], radiotherapy [16], and radiofrequency ablation [17] *are* commonly used to prolong the *patients*' survival time. Compared to these conventional approaches, laser-induced

* Corresponding author. Tel.: +86 21 65982586; fax: +86 21 65988653.
E-mail address: mqchu98@tongji.edu.cn (M. Chu).

0142-9612/$ – see front matter © 2013 Elsevier Ltd. All rights reserved.
http://dx.doi.org/10.1016/j.biomaterials.2013.01.086

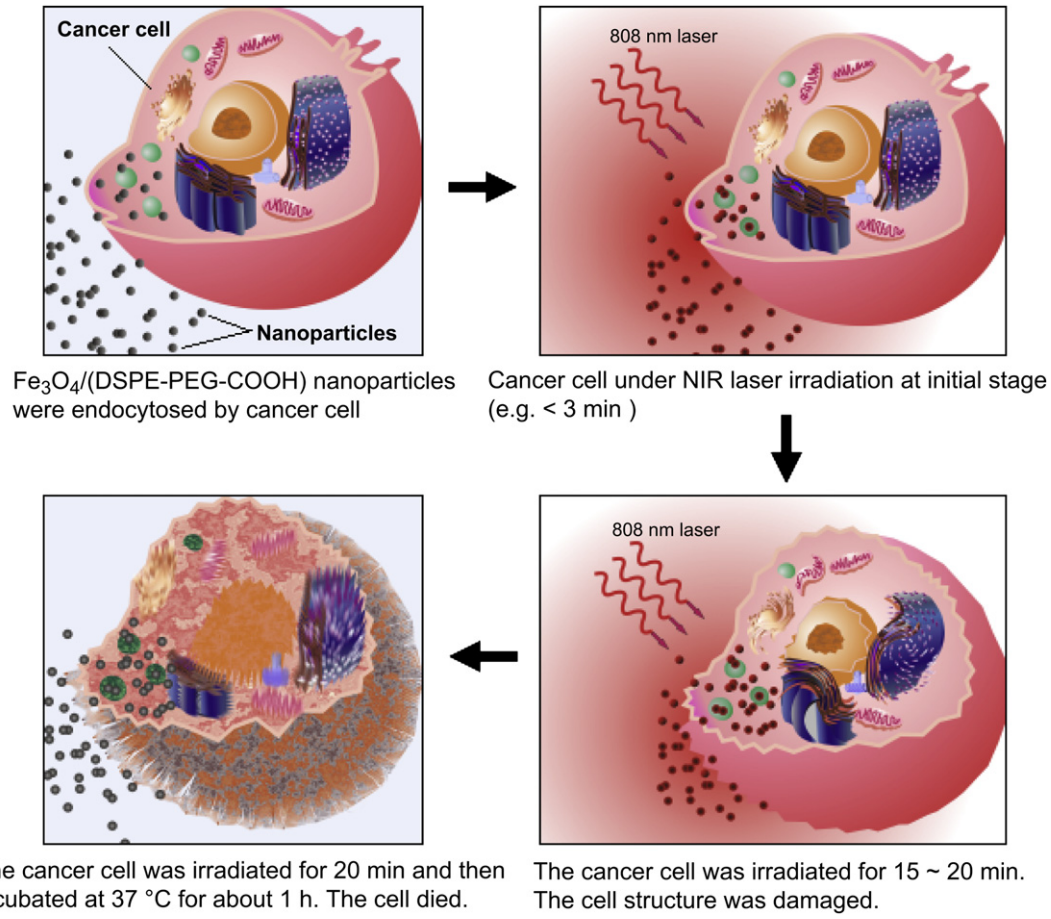

Fig. 1. Schematic illustrate of Fe_3O_4 nanoparticles coated with carboxyl-terminated poly (ethylene glycol)-phospholipid killing a cancer cell upon NIR laser irradiation.

photothermal hyperthermia via Fe_3O_4 nanoparticles may show a much higher energy conversion efficiency. Furthermore, Fe_3O_4 photothermal therapy may present great advantages as NIR light has an extensive safety profile in disease diagnostics and therapy.

2. Materials and methods

2.1. Materials

2.1.1. Reagents & materials

Oleic acid, sodium oleate and 1-octadecene were purchased from Sigma–Aldrich Corporation. Other chemical reagents such as $FeCl_3 \cdot 6H_2O$, $FeCl_2 \cdot 4H_2O$, $FeSO_4 \cdot 7H_2O$, $NH_3 \cdot H_2O$, NaOH, $NaNO_3$, H_2SO_4, OSO_4, epoxide resin, uranyl acetate, lead citrate, glutaraldehyde, ethanol and acetone etc., were purchased from Shanghai Chemical Regent Co. The RPMI-1640 culture medium and fetal calf serum (FCS) were obtained from Gibco (Carlsbad, CA, USA).Cell Titer-Glo® luminescent cell viability assay reagents were purchased from Promega Corporation (Madison, WI, USA).*Distearoyl-N-*[3-*carboxypropionoyl poly(ethylene glycol) succinyl*] *phosphatidylethanolamine* (DSPE-PEG_{2000} carboxylic acid, DSPE-PEG-COOH) was purchased from Avanti Polar Lipid, Inc., (Alabaster, AL, USA).

2.1.2. Cell lines and animal

Human esophagus carcinoma cells (Eca-109) were purchased from the Shanghai Institutes for Biological Sciences, Chinese Academy of Sciences (Shanghai, China). Nude mice (6–7 weeks old; BALB/c) were purchased from the Shanghai Sipper-BK Lab Animal Co. Ltd. (Shanghai, China), and were used in accordance with approved institutional protocols established by the Shanghai Department of Experimental Animals Management.

2.2. Methods

2.2.1. Synthesis of Fe_3O_4 nanoparticles

2.2.1.1. Spherical Fe_3O_4. These nanoparticles were synthesized by co-precipitation of iron chloride salts with ammonia [18]. For a typical synthesis, $FeCl_3 \cdot 6H_2O$ (4.43 g) and $FeCl_2 \cdot 4H_2O$ (1.625 g) were dissolved in distilled water (190 mL) by mechanical stirring at 60 °C in a three-necked round-bottom flask protected by nitrogen atmosphere flow. Under conditions of vigorous stirring, $NH_3 \cdot H_2O$ (10 mL, 25%) was poured into the vortex of the iron solution. After stirring for 30 min, the solution was precipitated by centrifugation and the black precipitates obtained were washed three times with ethanol and water, then redispersed in water sealed by nitrogen atmosphere.

2.2.1.2. Hexagonal Fe_3O_4. These nanoparticles were synthesized by a thermal decomposition method as previously described [19]. Briefly, the iron–oleate complex was prepared first by exposing iron chlorides and sodium oleate to 70 °C. 36 g of the resulting iron–oleate was then dissolved in 200 g of 1-octadecene and heated to 320 °C for 30 min. The solution was gradually cooled to room temperature and the precipitates were washed with ethanol 7–10 times to remove the excess oleate.

2.2.1.3. Wire-like Fe_3O_4. These nanoparticles were synthesized following the method described in Ref. [20] with a small modification. Briefly, NaOH (1.4 g) and $NaNO_3$ (4.25 g) powders were dissolved in a mixture solution containing 90 mL of water and 90 mL of ethanol. 20 mL of $FeSO_4 \cdot 7H_2O$ (2.78 g) aqueous solution containing 10 mmol/mL H_2SO_4 was then slowly added to the above solution under stirring and nitrogen atmosphere flow protection. The reaction was performed in a three-necked round-bottom flask. After the addition of $FeSO_4 \cdot 7H_2O$, the flask was sealed and heated to 90 °C in a thermostatic water bath for 24 h. The solution was gradually cooled to room temperature and the precipitate was washed three times with ethanol and water.

2.2.2. Studies on characterizations of Fe_3O_4 nanoparticles

The Fe_3O_4 shapes were studied by using a high-resolution transmission electron microscope (HRTEM) (JEOL-2010, Japan) operating at 200 kV. Sizes of the Fe_3O_4 nanostructures were determined by HRTEM over 120 particles for each sample, using the software provided with the HRTEM system. XRD patterns were taken on a diffractometer (4654-2A1; LCCAS, Japan) using a Ni-filtered Cu Kα ($\lambda = 0.154$ 18 nm) radiation. The room-temperature magnetic properties were measured on a vibrating-sample magnetometer (a Physical Property Measurement System from Quantum Design, USA) with a maximum applied field of 1.8 T. The absorption spectra were

taken on a diode array spectrophotometer (UV-2102PC; Unico, Shanghai, China) with a deuterium lamp source.

2.2.3. Photothermal effect measurements

The Fe_3O_4 nanoparticles were precipitated from aqueous solutions, and freeze-dried for 48 h using a freeze-dryer (Christ Alpha-2-4, Osterode, Germany). The dry powders obtained (~6 mg) were placed inside the polyethylene plastic bags at the corners (thickness: ~0.03 mm). Three lasers (Shanghai Inter-Diff Optoelectronics Tech. Co., Ltd., Shanghai, China) respectively with wavelengths of 655 (power density, 0.5 W/cm^2; spot area, 5 × 8 mm), 671 (power density, 0.2 W/cm^2; spot area, 9 × 9 mm), and 808 nm (power density, 0.25 W/cm^2; spot area, 5 × 8 mm) were used to irradiate the Fe_3O_4 nanoparticle powders through the thin plastic film at room temperature. As a control, the plastic bag film alone was irradiated with the same lasers as described above. The heat damage of the plastic films was monitored by a digital color camera (Nikon Coolpix 4300; Nikon, Tokyo, Japan).

To accurately monitor the temperature changes in Fe_3O_4 samples upon laser irradiation, the Fe_3O_4 nanoparticles were surface-modified with DSPE-PEG-COOH. For a typical experiment of surface modification, DSPE-PEG-COOH powder (8–10 mg) was dissolved in chloroform (1 mL) in a round-bottomed flask and dried via rotary evaporation to make a thin film. The film was then blown dry with nitrogen to remove chloroform. The Fe_3O_4 nanoparticle aqueous suspension (1 mL, 8 mg/mL) was added into the flask to hydrate the dry lipid film. The mixture suspension was gently shaken for 2 h, and then sonicated for approximately 30 min under nitrogen. For Fe_3O_4 nanoparticle suspensions of different concentrations, Fe_3O_4/(DSPE-PEG-COOH) was diluted with water to obtain solutions containing 0.8 and 0.08 mg/mL of Fe_3O_4, respectively.

Fe_3O_4/(DSPE-PEG-COOH) aqueous suspensions with different Fe_3O_4 concentrations (0.08, 0.8 and 8 mg/mL; 200 μL for each sample) were placed in small transparent glass tubes (wall thickness: ~0.5 mm; inner diameter: ~6 mm; height: 2 cm). The open ends of the tubes were covered with a sealing film (Whatman, Kent, UK) after the suspensions were added. The sealing film centers were poked with a 1 mm diameter orifice for insertion of the induction probe (0.25 mm in diameter, made by our research group) of a chromel-Alumel thermocouple thermometers (Shanghai Instrument Factory Co., Ltd., Shanghai, China). The baseline temperature was maintained at 25 ± 0.2 °C. The 655, 671 and 808-nm lasers were respectively used to irradiate the solutions for 3, 5, 10, 15 or 20 min. At each time point, the laser was shut off and the probe of the thermocouple thermometer was immediately inserted into the suspensions through the orifice in the sealing film. As controls, the temperatures of distilled water (200 μL) irradiated by the same lasers as described above were measured. All experiments were conducted in triplicate.

2.2.4. In vitro photothermal therapy

Firstly, we used a laser-scanning confocal microscope (TCS NT: Leica, Nussloch, Germany) to directly observe cell morphologies after the cells were treated with Fe_3O_4/(DSPE-PEG-COOH) nanoparticles and laser irradiation. The Eca-109 cells were seeded in 10 × 10 mm dishes and incubated with 200 μL of RPMI-1640 medium containing Fe_3O_4/(DSPE-PEG-COOH) nanoparticles with spherical, hexagonal, and wire-like Fe_3O_4 cores at 37 °C. The concentration of the Fe_3O_4 was 0.5 mg/mL. The cells were irradiated with the 808-nm laser for 3, 15 and 20 min and continuously incubated at 37 °C for 0 and 60 min and then imaged with the microscope. As controls, the cells incubated with the same amount of magnetic nanoparticles as described above without laser irradiation, and the cells alone with and without laser irradiation were also imaged with the microscope.

Secondly, we used the Cell Titer-Glo reagent to quantitatively detect the cell viability. Eca-109 cells were seeded into 96-well plates (100 μL for each well) with 5% $CO_2$and cultured at 37 °C in an RPMI-1640 medium containing 10% FCS and 1% antibiotic-antimycotic. Only three wells from each 96-well plate were seeded with cells. After incubation for 24 h, the culture medium was removed, and one well was added with culture medium and other two wells were added with medium containing Fe_3O_4/(DSPE-PEG-COOH) nanoparticles of different Fe_3O_4 concentrations (0.1, 0.5 and 1 mg/mL; 100 μL for each well). Only one well of cells incubated with the nanoparticles were then irradiated with the 808 nm laser for 20 min at 37 °C inside the incubator. After irradiation, all the cells were continually cultured at 37 °C for 1 h. The culture medium was then removed and the cells were gently washed with PBS. After washing, CellTiter-Glo reagent (100 μL, Promega Corporation, Beijing, China) was immediately added to the cells, then gently shaken for 2 min to induce cell lysis and incubated at room temperature for 10 min. The adenosine triphosphate (ATP) luminescent intensities of cells were measured using a SpectraMax M5 Universal Microplate Spectrophotometer (Molecular Devices Inc., California, USA). All experiments were conducted for five times. Cell viability was calculated by a luminescent assay based on the quantization of ATP present in cells.

Finally, the cell structures were analyzed with TEM images. For a typical experiment, the cells were gently washed two times with PBS, and then collected by trypsin digestion. After addition of several drops of 2.5% glutaraldehyde, the cell suspensions were precipitated by centrifugation. 0.5 mL of 2.5% glutaraldehyde was then added into each cell precipitate sample and they were fixed at 4 °C overnight. The 2.5% glutaraldehyde was then replaced by 0.1 M PBS (pH 7.3), followed by postfixation with 1% OSO_4 solution at 4 °C for 2 h and three times washing with PBS (15 min for each wash). The cells were dehydrated at 4 °C in a series of ethanol solutions (50%, 70% and 90%) and 1:1 mixture solution of ethanol (90%):acetone (90%) (15–20 min for each solution). The cells were continually dehydrated in a series of acetone solutions (90% (one time at 4 °C), 100% (three times at room temperature)) (15–20 min for each time). Afterwards, the cells were treated with a 2:1 mixture solution of acetone:epoxide resin for 3 h, and treated with a 1:2 mixture solution of acetone:epoxide resin overnight. The cells were then embedded in pure epoxide resin, which were polymerized at 37 °C (overnight), 45 °C (12 h) and 60 °C (48 h), respectively. The ultrathin sections of the embedded specimens were cut with an ultramicrotome (Lecia EM uc6) using a diamond knife. The thin sections were placed onto formvar/carbon-coated copper grids and stained with 3% uranyl acetate and lead citrate, respectively. The sections were then examined by a TEM (JEOL, JEM-1400, Japan) at an accelerating voltage of 80 kV. The elements of Fe_3O_4 in cells were analyzed using an energy dispersive X-ray spectrometry (EDS)(OXFORD) analysis system.

2.2.5. The retention of the Fe_3O_4 nanoparticles in the tumor sites

Five mice were injected subcutaneously in the right side with Eca-109 cells (~1 × 10^6). Three weeks after implantation, the mice tumors were resected and sliced into pieces (~1 × 1 mm) and replanted in the right sides of 60 mice. Approximately ten days after implantation, nine mice with similar tumor sizes (length ≈ width ≈ 6–7 mm) were selected for the studies of the retention of Fe_3O_4 nanoparticles in the tumor sites.

The tumor-bearing mice were injected with 60 μL of PBS-dispersed Fe_3O_4/(DSPE-PEG-COOH) (Fe_3O_4: 8 mg/mL) and sacrificed on day 1, 3 and 24 after injection, respectively. Three mice were randomly selected and sacrificed at each time point and the tumors were extracted immediately after. The tumors were weighed, immersed in 0.5 mL of distilled water containing several small glass beads and ground into a mash using a tissue grinder (Mini bead-beater™, Biospec products, USA). Afterwards, the tissue mashes were mixed with 0.5 mL of aqua regia and incubated at room temperature. A week later, the samples were centrifuged and the upper clear solutions were collected and adjusted to 9 mL with distilled water. The concentrations of Fe atoms in these solutions were measured using the inductively-coupled-plasma atomic-emission spectrometry (ICP-AES)(iCAP6300, Thermo Jarrell Ash Co., Franklin, MA, USA).

2.2.6. Photothermal therapy in vivo

30 mice with similar tumor sizes (length ≈ width ≈ 4–5 mm) were selected from the above 60 tumor-bearing mice for the photothermal therapy. The mice were separated into six groups ($n = 5$ per group), and 70 μL of PBS, PBS-dispersed Fe_3O_4/(DSPE-PEG-COOH) (Fe_3O_4: 8 mg/mL) or DSPE-PEG-COOH (5 mg/mL) were locally injected into the tumors. Each type of solution (or suspension) was injected into 10 mice. In the three irradiation groups, the tumors injected with PBS, Fe_3O_4/(DSPE-PEG-COOH) or DSPE-PEG-COOH were irradiated with the 808 nm laser, with each mouse irradiated for 20 min every 24 h. The remaining three groups injected with PBS, Fe_3O_4/(DSPE-PEG-COOH) or DSPE-PEG-COOH were not laser irradiated. The tumor morphologies were recorded with a digital color camera during the treatment. The tumor sizes were measured at the widest width and along the perpendicular length using a caliper. The tumor volumes were calculated based on the following formula: $V = L \times W^2/2$. In this equation, V, L and W are tumor volume, length, and width, respectively. The tumor volume was regarded as 'zero' at its disappearance.

2.2.7. Histological analysis of tumor tissues

Into two tumor-bearing mice (tumor length ≈ width ≈ 6–7 mm) 70 μL of PBS-dispersed Fe_3O_4/(DSPE-PEG-COOH) containing 8 mg/mL of Fe_3O_4 nanoparticles was intratumorally injected, and one mouse tumor was then irradiated with the 808-nm laser for 20 min every 24 h, while the other one was not irradiated. Four days after irradiation and/or injection, the mice were killed and the tumors were resected. The fresh tumor tissues were fixed 24 h in 4% paraformaldehyde at 4 °C, and then embedded in paraffin after tissue processing. The paraffin ultrathin sections of the embedded specimens were cut with an ultramicrotome (Lecia EM uc6); and the thin sections were placed onto glass slides and stained with hematoxylin and eosin staining (H & E staining) to analyze the tissue structure and cell state. The section samples were also stained with terminal deoxynucleotidyl transferase biotin-dUTP nick-end labeling (TUNEL assay) to detect apoptotic or necrotic cells. As a control, a tumor-bearing mouse injected with PBS without irradiation was killed, and the tumor tissue was then cut and stained the same way as described above. Images of the tissue sections were obtained using an upright digital microscope (DM 4000: Leica, Nussloch, Germany).

The tumor tissues were also prepared for TEM imaging and EDS analysis. The fixing, embedding, ultrathin cutting, observation and analysis methods were the same as those described above (see the cell experiments).

2.2.8. Statistical analysis

Statistical significance was determined by analysis of variance (ANOVA) followed by Tukey's post hoc test, and a P-value < 0.05 was considered statistically significant; $P < 0.01$ was considered highly significant.

3. Results and discussion

3.1. Properties of Fe_3O_4 nanoparticles with three shapes

The magnetic Fe_3O_4 nanoparticles of spherical, hexagonal and wire-like shapes were synthesized in this study by the chemical routes described in the Methods section. HRTEM images show that the dimensions of the spherical and hexagonal Fe_3O_4 nanoparticles are 9.1 ± 1.9 and 9.4 ± 1.3 nm, respectively, while that of the wire-like Fe_3O_4 particles is 12.6 ± 5.9 nm in diameter and several hundred nanometers (or several micrometers) in length (Fig. 2A). All these nanoparticles are shown to have a face-centered cubic phase (Fig. 2B) and superparamagnetic properties (Fig. 2C). Their aqueous suspension shows a broad and continuous absorption spectrum and the NIR absorption intensity increases with increasing concentration of Fe_3O_4 (Fig. 2D). NIR absorption is ideal for *in situ* cancer photothermal therapy due to its in-depth tissue penetration.

3.2. Photothermal conversion of Fe_3O_4 nanoparticles

The photothermal conversion effect was initially studied on dry Fe_3O_4 nanoparticle powders, which were placed inside the corners of polyethylene plastic bags and exposed to 655, 671, and 808 nm lasers as schematically shown in Fig. 3A. Upon laser irradiation, the dry powder generates sufficient heat and rapidly burns out a considerable area of the plastic film that is directly in contact with the powder within only approximately 20 s, as shown in Fig. 3B. The heat-damaged area at 655 nm laser induction appears larger than

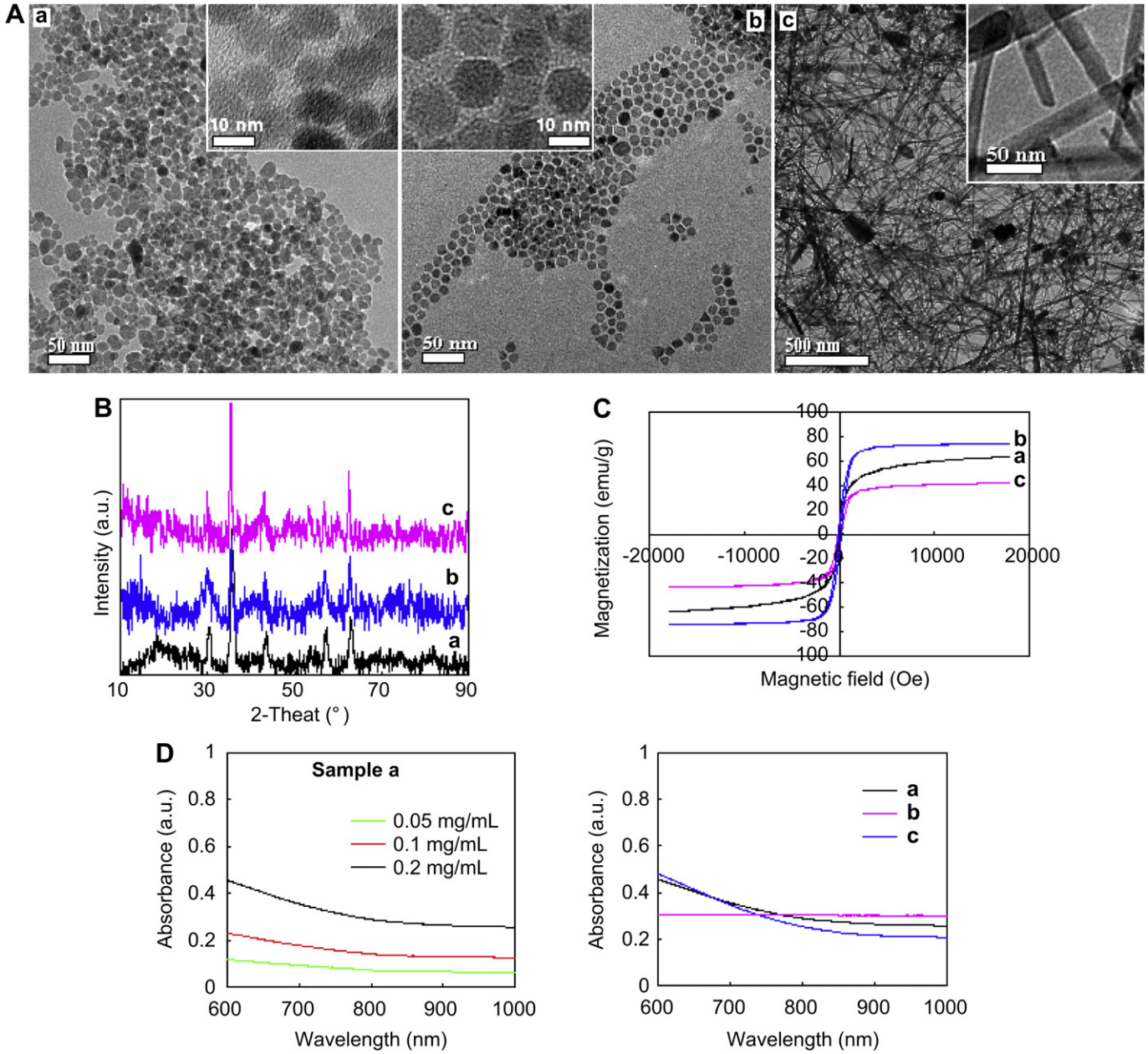

Fig. 2. Fe_3O_4 nanoparticles. (A) HRTEM images of spherical, hexagonal, and wire-like Fe_3O_4 nanoparticles. (B) and (C) are XRD patterns and magnetization of the nanoparticles shown in (A), respectively. (D) Absorption spectra of the spherical Fe_3O_4 nanoparticles in different concentrations (left), and spherical and hexagonal and wire-like Fe_3O_4 nanoparticles containing 0.2 mg/mL of Fe_3O_4 (right).

those after 671 and 808 nm irradiation, indicating a more pronounced photothermal effect at a shorter wavelength. However, the plastic film remains undamaged without Fe_3O_4 powder when exposed to laser irradiation for the same time period, as shown in Fig. 3C. No obvious differences in photothermal effects were found among the spherical, hexagonal, and wire-like Fe_3O_4 nanoparticles. These results indicated sufficient photothermal effects of Fe_3O_4 nanoparticles activated by red and NIR laser irradiation.

In order to characterize the photothermal effects of the water-dispersed samples, the Fe_3O_4 nanoparticles were functionalized with DSPE-PEG-COOH. The surface coating of DSPE-PEG-COOH provides the Fe_3O_4 nanoparticles with hydrophilic groups and spatial obstruction for improved dispersion in water. The DSPE-PEG-COOH coated-Fe_3O_4 nanoparticles [Fe_3O_4/(DSPE-PEG-COOH)] dispersed in aqueous solution (200 μL) are found to exhibit high photothermal converting efficiency (Fig. 4). At a concentration of only 0.08 mg/mL of spherical Fe_3O_4 nanoparticles, the temperature increase of the suspension is greater than 7 °C for 3 min, and 13 °C for 10 min after 808-nm laser irradiation (Fig. 4A). The temperature increase effect is more rapid at higher Fe_3O_4 nanoparticle concentrations. For example, at concentrations of 0.8 and 8 mg/mL, the temperature increases are respectively greater than 25 °C and 28 °C for 10 min post-irradiation with an 808-nm laser (Fig. 4A). The temperature increases are rapid in the first five minutes for all nanoparticle concentrations, but gradually leveled off thereafter. These results indicate a rapid high energy conversion efficiency in the Fe_3O_4 aqueous suspension.

For the spherical Fe_3O_4 nanoparticle (0.8 mg/mL) solutions, irradiated at shorter irradiation wavelengths (655 nm, 671 nm, 20 min), the temperature increases are 2–4 °C greater than those irradiated by the 808-nm laser (Fig. 4B), which is due to greater absorption at shorter wavelength. The photothermal conversion effects of both hexagonal and wire-like Fe_3O_4 nanoparticle suspensions upon 808-nm laser irradiation are found to be similar to that of the spherical Fe_3O_4 particles (Fig. 4C), attributable to their comparable absorptions at around 808 nm wavelength (Fig. 2D).

As controls, the temperature of distilled water irradiated by the 655, 671 and 808-nm lasers changed with a maximum temperature

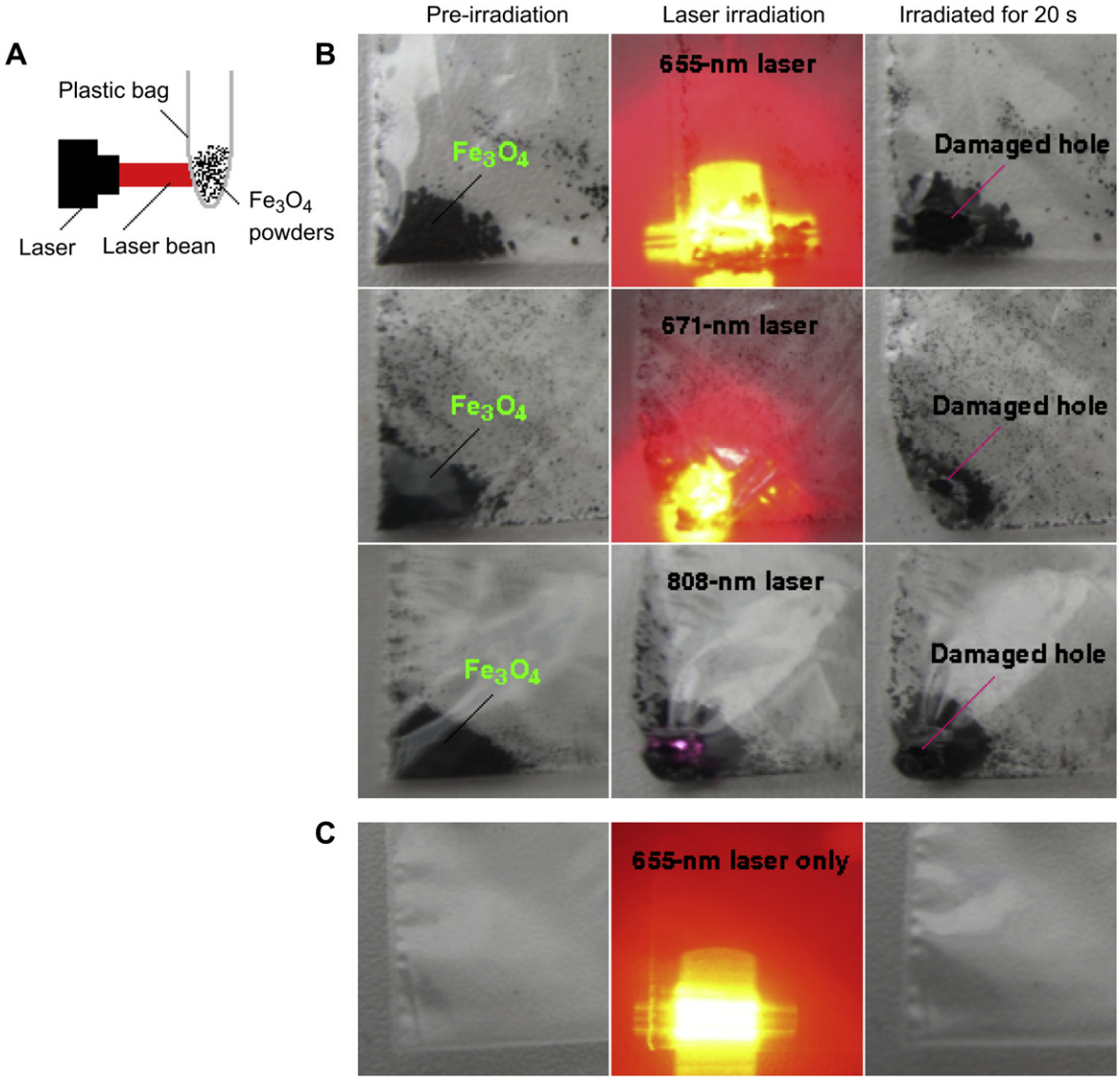

Fig. 3. Photothermal effect of spheric Fe_3O_4 nanoparticle dry powders induced by 655, 671 and 808 nm laser irradiation. (A) Schematic diagram of the polyethylene plastic bags (thickness: ~0.03 mm) loaded with Fe_3O_4 nanoparticle powder upon laser irradiation; (B) The plastic film is melted by the Fe_3O_4 nanoparticles after 20 s laser irradiation, and (C) The film remains undamaged after 655 nm laser irradiation without Fe_3O_4 nanoparticles (The undamaged films treated with the 671- and 808-nm laser irradiation without Fe_3O_4 nanoparticles are not shown).

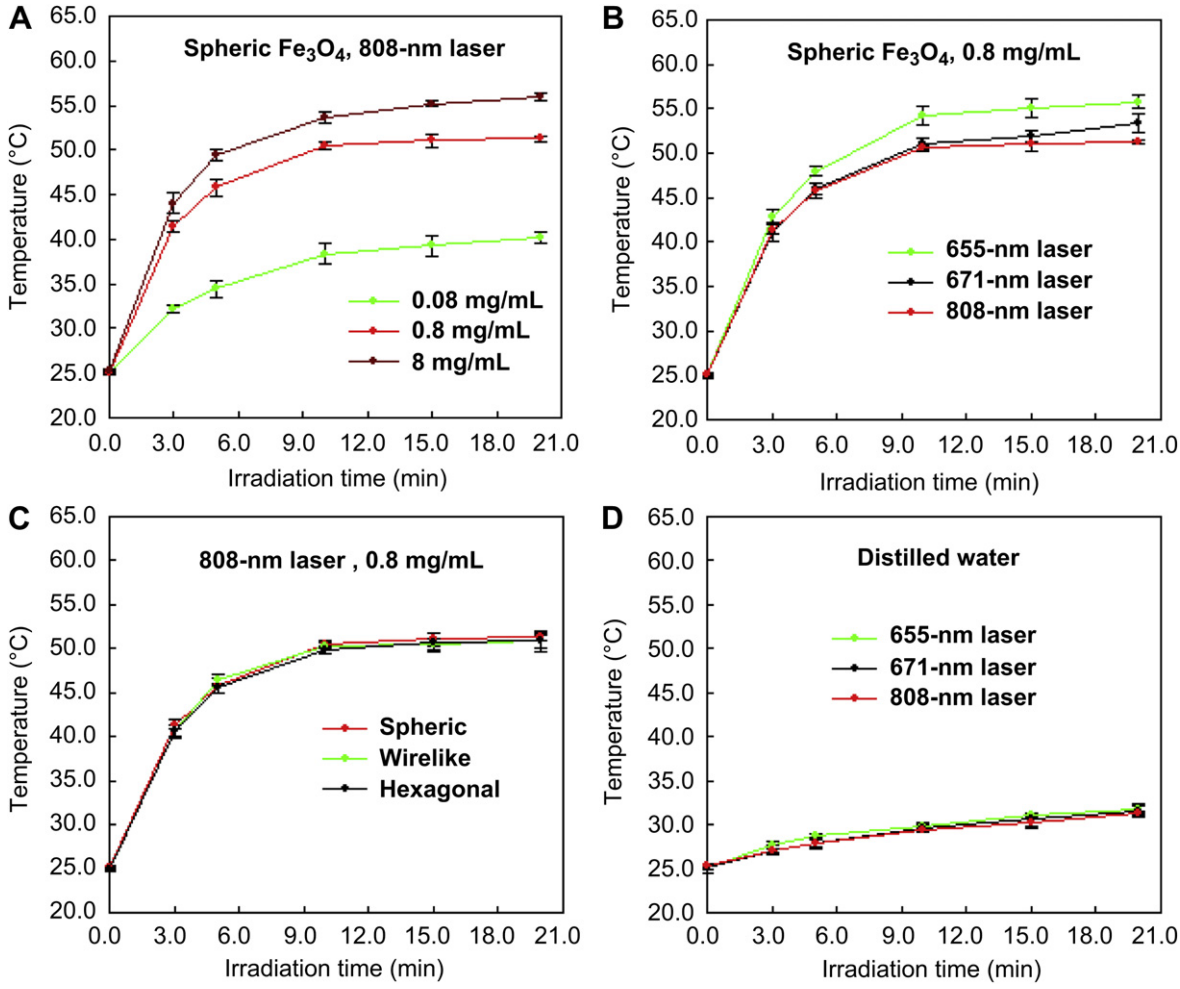

Fig. 4. Temperature vs. irradiation time of the aqueous suspensions of Fe_3O_4 nanoparticles with different concentrations and indicated shapes, including distilled water. Irradiation was done with 655, 671, and 808 nm lasers, respectively. (A) Spherical Fe_3O_4 nanoparticles with different concentrations (0.08, 0.8 and 8 mg/mL) upon 808 nm laser irradiation; (B) Spherical Fe_3O_4 nanoparticles containing 0.8 mg/mL of Fe_3O_4 upon laser irradiation at 655, 671, and 808 nm, (C) Fe_3O_4 nanoparticles with spherical, hexagonal, and wire-like shapes, all containing 0.8 mg/mL of Fe_3O_4 upon 808 nm laser irradiation, and (D) Distilled water upon laser irradiation at 655, 671, and 808 nm. All Fe_3O_4 nanoparticles were coated with DSPE-PEG-COOH. All suspension volumes were 200 μL including distilled water. Error bars were based on standard deviations.

increase of no more than 6.7 °C after 20 min irradiation (Fig. 4D). This sharp contrast is a strong evidence of the photothermal effect found in Fe_3O_4.

3.3. Photothermal therapy in vitro using the Fe_3O_4 nanoparticles

TheFe_3O_4/(DSPE-PEG-COOH) nanoparticles with 0.5 mg/mL of spherical, hexagonal, and wire-like Fe_3O_4 cores were incubated with esophageal cancer cells (Eca-109) in culture medium and irradiated by the 808-nm laser. When the cells incubated with the nanoparticles were irradiated only about 3 min and continuously incubated at 37 °C for 60 min, most of the cell retained healthy appearance (data not shown). However, when the cells were irradiated for 20 min and then continuously incubated at 37 °C for 60 min, the bright field microscope images (Fig. 5) showed that more than half of the cells were significantly shrunken and exhibited unhealthy appearance. It should be noted that if the cells were irradiated for 20 (or 15) min and then immediately observed using the microscope, the cells were also shrunken some but the volumes of the cells were larger than those of the cells shown in Fig. 5 (data not shown). In contrast, the morphologies of cells incubated with magnetic nanoparticles without laser irradiation and the morphology of cells with solely irradiation did not obviously change. This implies that the cells incubated with magnetic nanoparticles may have been damaged or killed after about 20 min laser irradiation, whereas, the cell viability may have been not influenced by solely magnetic nanoparticle application or laser irradiation.

The results of a quantitative cell cytotoxicity assay determined by the Cell Titer-Glo luminescent cell viability, showed that the Eca-109 cell viability significantly decreased to 52.16 ± 12.30% after the cells were incubated with Fe_3O_4/(DSPE-PEG-COOH) particles containing 0.5 mg/mL of spherical Fe_3O_4 cores and 20 min 808-nm laser irradiated and continuously incubated at 37 °C for 60 min (Fig. 6A). The cell viability was well scaled with the concentration of Fe_3O_4 nanoparticles, upon irradiation. For example, the cell viabilities was 40.16 ± 4.14% and 83.37 ± 10.01% for the Fe_3O_4 concentrations of 1 and 0.1 mg/mL, respectively (Fig. 6A). The hexagonal and wire-like Fe_3O_4 nanoparticles exhibited similar cell killing abilities upon NIR irradiation. As shown in Fig. 6B, the cell viabilities were 54.25 ± 4.29% and 51.54 ± 4.78% for the hexagonal and wire-like Fe_3O_4 nanoparticles (containing 0.5 mg/mL of Fe_3O_4), irradiated by the NIR laser for 20 min.

However, for the same groups without irradiation, no obvious cell viability change was observed and in the cell-alone experiment, no significant decrease in cell viability was observed when irradiated by the laser (Fig. 6A). These results indicate distinctive photothermal effects of Fe_3O_4 nanoparticles on cell growth, and minimal effects of laser irradiation without the particles.

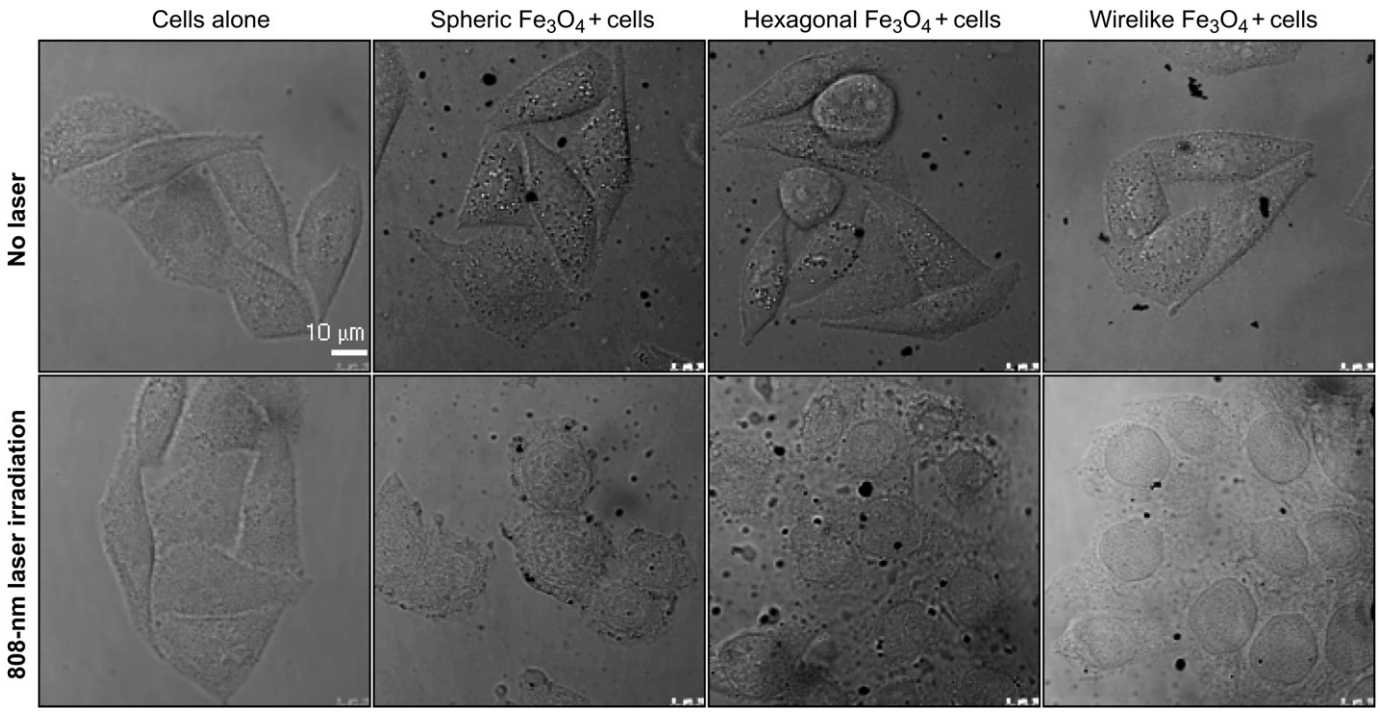

Fig. 5. Bright field images of Eca-109 cells and Eca-109 cells incubated with Fe_3O_4/(DSPE-PEG-COOH) nanoparticles with spherical, hexagonal, and wire-like shapes, all containing 0.5 mg/mL of Fe_3O_4 without (up panels) and with (bottom panels) 808-nm laser irradiation. For the irradiation group, the cells were irradiated for 20 min, and then continuously incubated at 37 °C for 60 min. For the non-irradiation group, the cells were incubated at 37 °C for 80 min. The images were taken using a confocal laser-scanning microscope using a 63 × oil objective lens.

The details of Eca-109 cell structures destroyed by the photothermal effects of Fe_3O_4 nanoparticles can be observed by TEM images. For the cells incubated with the Fe_3O_4/(DSPE-PEG-COOH) nanoparticles (containing 0.5 mg/mL of Fe_3O_4) for 80 min without laser irradiation, the structures of nucleus and organelles were intact. The cell membrane and nuclear membrane remained integral, the mitochondria (several with tubular cristae) and endoplasmic reticulum exhibited their original normal appearance, and the Fe_3O_4 nanoparticles were endocytosed by the cells, which could be clearly observed by the TEM (Fig. 7A, upper panels) and confirmed by the EDS (Fig. 7B, upper panel). For the cells incubated with the nanoparticles after 20 min of 808-nm laser irradiation, the Fe_3O_4 nanoparticle aggregations inside the cells also could be observed by the TEM (Fig. 7A, bottom panels) and confirmed by the EDS (Fig. 7B, bottom panel). However, the organelle structures became illegibility or disappeared, and the nuclear membrane has been destroyed (Fig. 7A, bottom panels). These results indicate that the Fe_3O_4/(DSPE-PEG-COOH) nanoparticles can be uptaken by cancer cells, and these nanoparticles without laser irradiation have no or low toxicity to cells, whereas, upon laser irradiation, the cell structures are seriously damaged by the photothermal effects of the nanoparticles.

3.4. Tumor retention of the Fe_3O_4 nanoparticles and photothermal therapy in vivo

For more in-depth penetration in tumors, an NIR laser of 808 nm was employed to conduct the animal studies. The Fe_3O_4/(DSPE-

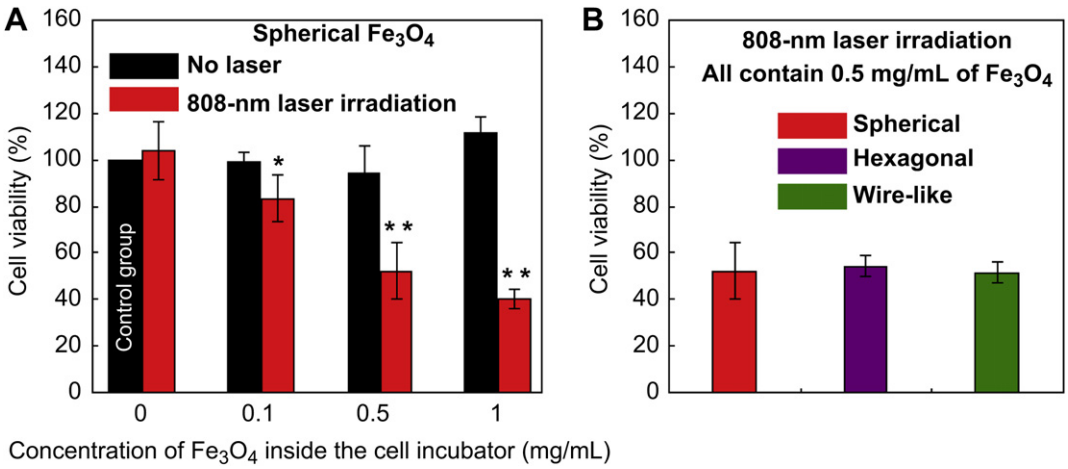

Fig. 6. Effects of Fe_3O_4/(DSPE-PEG-COOH) on esophageal cancer cell viability with or without 808-nm laser irradiation. (A) Spherical Fe_3O_4 nanoparticles with different concentrations (0, 0.1, 0.5 and 1 mg/mL), with or without irradiation. (B) Fe_3O_4 nanoparticles with spherical, hexagonal, and wire-like shapes, all containing 0.5 mg/mL of Fe_3O_4 upon irradiation. The significance levels observed are $^{*}P < 0.05$ and $^{**}P < 0.01$ in comparison to control group values. Error bars were based on standard deviations.

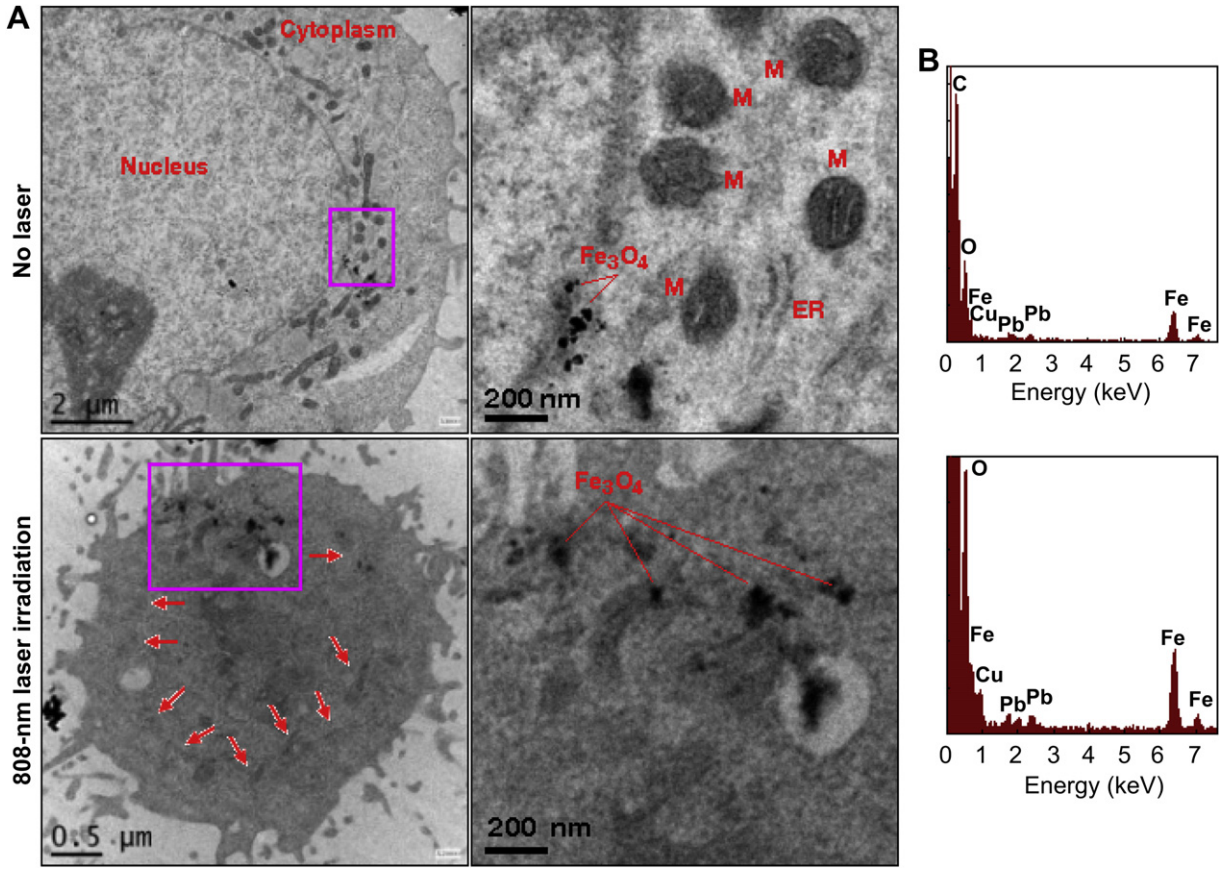

Fig. 7. (A) TEM images and (B) EDS spectra of ultrathin sections of Eca-109 cells incubated with Fe_3O_4/(DSPE-PEG-COOH) without and with 808-nm laser irradiation. The concentration of Fe_3O_4 was 0.5 mg/mL. The right figures of (A) are partial enlarged views of the pink panels shown in corresponding left figures of (A), and the EDS spectra are also of the red panels shown in corresponding left figures. For the irradiation group, the cells were incubated with the nanoparticles and irradiated with the laser for 20 min and then incubated at 37 °C for 60 min. For the non-irradiation group, the cells were incubated with the nanoparticles at 37 °C for 80 min. M indicates mitochondria, ER indicates endoplasmic reticulum. The traces pointed with the red arrows may be the damaged nuclear membrane. (The Fe_3O_4 nanoparticles used in this figure and the following figures were spherical in shape) (For interpretation of the references to color in this figure legend, the reader is referred to the web version of this article.).

PEG-COOH) nanoparticles of spherical geometry were used for the photothermal therapy. To investigate the retaining ability of the Fe_3O_4 nanoparticles, the ICP-AES was used to determine the iron atoms entrapped in the tumors. The results showed that 99.98 ± 32.72%, 79.17 ± 8.84%, and 74.49 ± 8.46% of Fe_3O_4 nanoparticles remained in the tumors for 1, 3 and 24 days post-injection (Fig. 8). A large amount of black Fe_3O_4 nanoparticles could be observed clearly on the tumor site even 24 days post-injection (Supplementary Fig. 1). The high long term Fe_3O_4 uptake is particularly important for photothermal cancer therapies as the irradiation period normally lasts for at least three weeks.

For an in vivo photothermal therapy, nude mice subcutaneously transplanted with human esophageal tumors on their right flanks were used. The mouse tumors were irradiated for 20 min every 24 h for 24 days using an 808 nm laser. As shown in Fig. 9, after mouse tumors were directly injected with 70 μL of PBS-dispersed Fe_3O_4/(DSPE-PEG-COOH) particles (Fe_3O_4: 8 mg/mL), followed by irradiation with the laser, the tumor growth was significantly suppressed. In addition, a charring spot appears on the tumor site (Fig. 9A, mouse on first line, Supplementary Fig. 2), indicating hemorrhage caused by photothermal heat generated by the Fe_3O_4 nanoparticles. In this irradiation group, one mouse tumor was completely eliminated on day 9 of irradiation.

In contrast, the tumors in the control animals injected with solely 70 μL of PBS or PBS-dispersed Fe_3O_4/(DSPE-PEG-COOH) particles (Fe_3O_4: 8 mg/mL) or DSPE-PEG-COOH (5 mg/mL) without

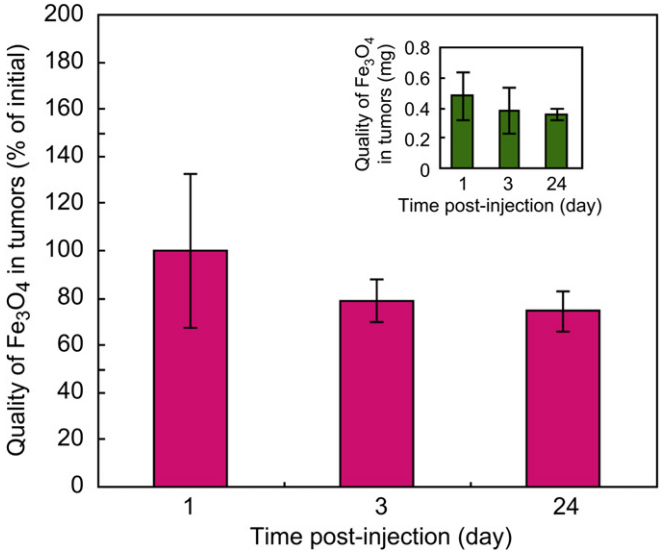

Fig. 8. Percentage of mass retention of Fe_3O_4 in tumors measured by ICP-AES. The tumor-bearing mice (n = 9) were intratumorally injected with Fe_3O_4/(DSPE-PEG-COOH) aqueous suspensions (insert: quality of Fe_3O_4 in tumors). Error bars were based on standard deviations according to three mice per group.

irradiation grow markedly over time, and the growth rates of these tumors were similar to those injected with PBS or PBS-dispersed DSPE-PEG-COOH with irradiation (Fig. 9B). In the control groups, no dark spots were observed in any tumor ($n = 25$) (Fig. 9A, mice on the second and third lines, Supplementary Figs. 3–7). These results clearly showed evidence of tumor growth inhibition by Fe_3O_4 photothermal therapy.

3.5. Histology analysis after the photothermal treatment of the Fe_3O_4 nanoparticles

Histology analysis of tumor tissues further demonstrated that the tumor cells are significantly destroyed by the Fe_3O_4 nanoparticles laser irradiation treatment. We examined tumor-bearing mice treated 4 days with 70 μL of PBS and PBS-dispersed Fe_3O_4/(DSPE-PEG-COOH) containing 8 mg/mL of Fe_3O_4 nanoparticles. When a mouse was intratumorally injected with the Fe_3O_4 nanoparticles and irradiated for 4 days (irradiated for 20 min every 24 h), the H & E staining results showed that the structure of tumor tissue was lost, and the cells in the tissue were shrunken with disappeared nuclei (Fig. 10A, right panel). However, for the tumors of mice intratumorally injected with PBS and magnetic nanoparticles without laser irradiation, the tissues exhibit a normal-organized cellular structure (Fig. 10A, middle and left panels). The tumor cell damage by the photothermal effect of Fe_3O_4/(DSPE-PEG-COOH) particles was also confirmed by TUNEL assays. Generally, the necrotic or apoptotic cells were stained brown, whereas, the robust and viable cells stained blue. As shown in Fig. 10B, many cells of the mouse tumor injected with the magnetic nanoparticles exhibited brown color staining after 4 days of laser irradiation, which

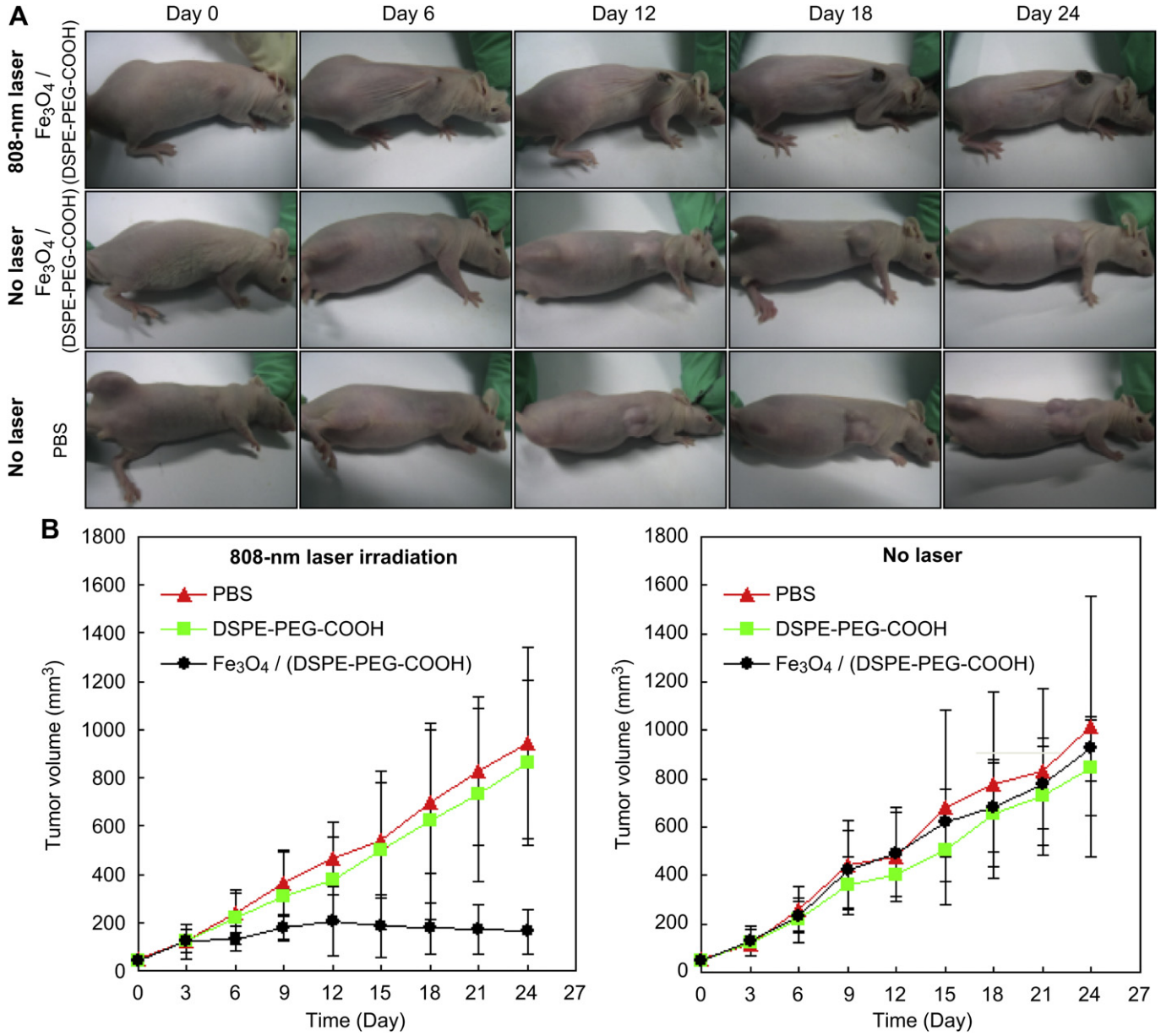

Fig. 9. Photographs and volumes of mouse tumors treated with 70 μL of PBS-dispersed Fe_3O_4/(DSPE-PEG-COOH) containing 8 mg/mL of Fe_3O_4, DSPE-PEG-COOH (5 mg/mL), and PBS alone with and without 808-nm laser irradiation. (A) Representative photos of tumors with and without laser irradiation; (B) Tumor growth curves with (left) and without (right) laser irradiation. Day 0 marks the tumor pre-irradiation and/or pre-injection, while day 3–24 mark the time periods from the first irradiation and/or injection. Photographs of all mice tumors ($n = 30$) with varying irradiation times are shown in Supplementary Figs. 2–7. Only the Fe_3O_4/(DSPE-PEG-COOH) and 808-nm laser treated group showed significant tumor growth suppression compared with the control group (PBS, no laser) ($P < 0.05$). Error bars were based on standard deviations.

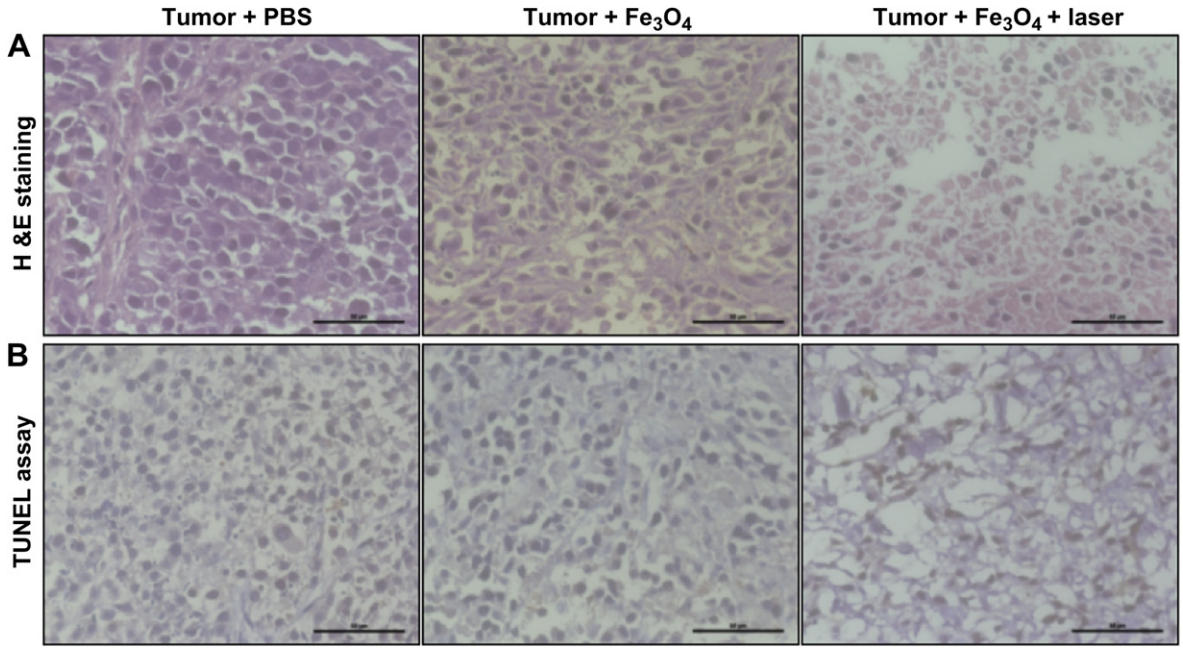

Fig. 10. Histologic assessments of tumor tissues with and without photothermal treatments of Fe_3O_4/(DSPE-PEG-COOH) nanoparticles and control. (A) H&E stained images; (B) TUNEL assay images. The tumor tissues were from PBS without laser treated group (left), Fe_3O_4/(DSPE-PEG-COOH) without laser treated group (middle), and Fe_3O_4/(DSPE-PEG-COOH) with 808-nm laser treated group (right), respectively. Scale bar: 50 μm.

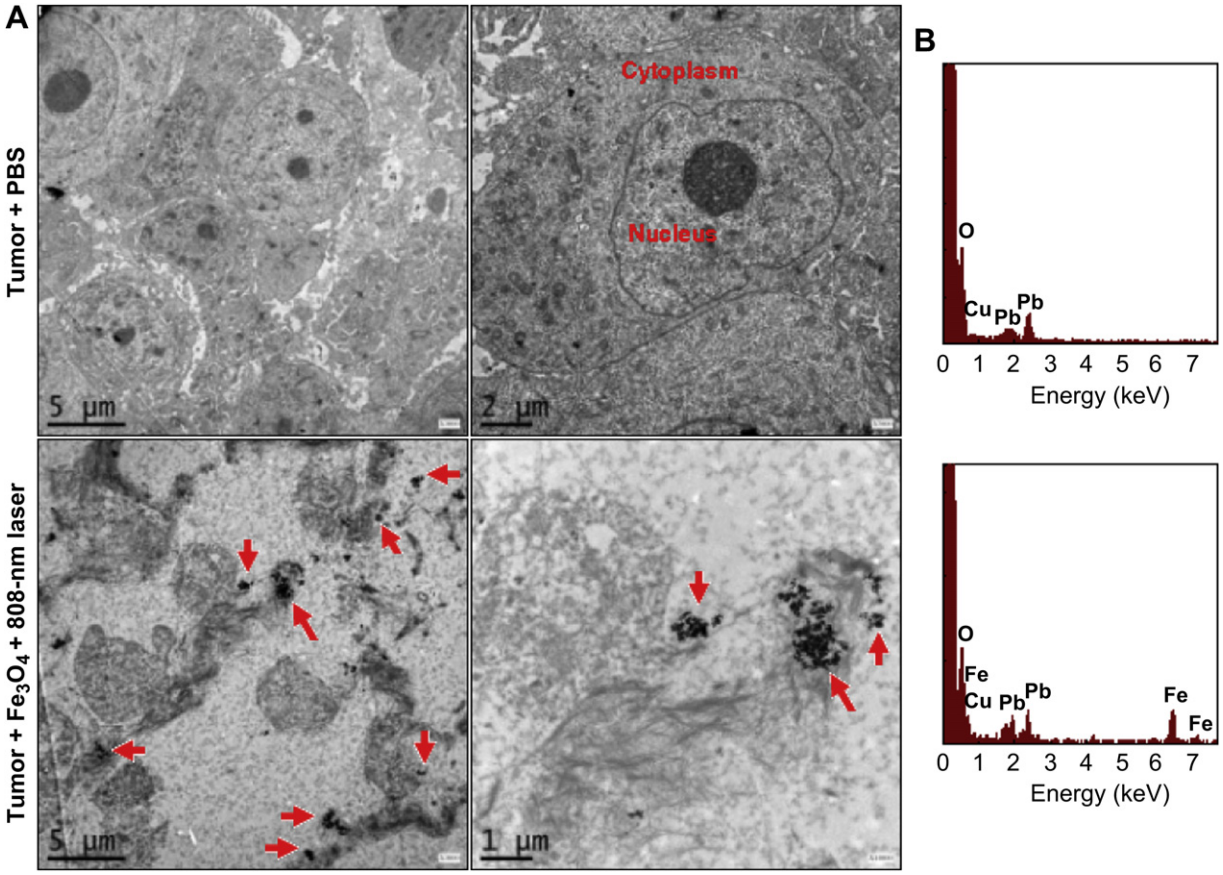

Fig. 11. (A) Typical TEM images of ultrathin sections of tumor tissues. Upper panels: the tumor of a mouse intratumorally injected with 70 μL of PBS without irradiation; bottom panels: the tumor of a mouse intratumorally injected with 70 μL of Fe_3O_4/(DSPE-PEG-COOH) containing 8 mg/mL of Fe_3O_4 after 808-nm laser irradiation for 4 days. The right figures are partial enlarged views of the same sections as shown in corresponding left figures. The arrows point to Fe_3O_4 nanoparticles. (B) EDS spectra of the sections shown in the corresponding panels shown in (A).

indicated that these cells have died or were apoptotic. Therefore, the growth of tumors synchronously treated with the magnetic nanoparticles and laser irradiation was clearly inhibited. However, the cells of mouse tumors injected with solely PBS or the magnetic nanoparticles without laser irradiation stained with blue color, which indicated that these cells were not affected.

TEM images of ultrathin sections further showed that the tumor tissues were seriously damaged when the mice were intratumorally injected with the Fe_3O_4/(DSPE-PEG-COOH) nanoparticles and treated 4 days with 808-nm laser irradiation. As shown in Fig. 11A, compared with the tumor tissue only injected with PBS, the tissue treated with the Fe_3O_4 nanoparticles and laser irradiation exhibited discontinuous structure with significantly shriveled cells, in which organelles vesiculated or disappeared, and some cells have finally disintegrated. The Fe_3O_4 nanoparticles were located in both intracellular and extracellular spaces, which could be confirmed by EDS analysis (Fig. 11B).

Other inorganic nanoparticles including carbon nanotubes [21], graphene [22], activated carbon [23], gold nanoparticles [24] and quantum dots [25] have been used for photothermal therapy, induced by NIR light irradiation. However, magnetic iron oxide nanoparticles have been used clinically, and numerous have already received Federal Drug Administration approval for clinical use [26].

4. Conclusions

Fe_3O_4 nanoparticles of various shapes have been found to exhibit strong photothermal effects, induced by red and NIR laser irradiation. It is demonstrated in this study that this photothermal effect is highly efficient for cancer therapy and in vitro experimental results showed significant suppression of cell viability. Using a human esophageal cancer model, the tumor growth was effectively inhibited by the NIR-induced hyperthermia of the spherical Fe_3O_4 nanoparticles. The photothermal effect of magnetic iron oxide may be well utilized as an efficient strategy in clinical cancer therapies.

Acknowledgments

The authors would like to gratefully acknowledged Dr. Alexander Endler for critically reading and revising the manuscript. This work was supported in part by the National Natural Science Foundation of China (81071833) and Natural Science Foundation of Jiangsu Province (SBK201123093).

Appendix A. Supplementary data

Supplementary data related to this article can be found at http://dx.doi.org/10.1016/j.biomaterials.2013.01.086.

References

[1] Zhang L, Xue H, Gao C, Carr L, Wang J, Chu B, et al. Imaging and cell targeting characteristics of magnetic nanoparticles modified by a functionalizable zwitterionic polymer with adhesive 3,4-dihydroxyphenyl-L-alanine linkages. Biomaterials 2010;31:6582–8.
[2] Lee JH, Jang JT, Choi JS, Moon SH, Noh SH, Kim JW, et al. Exchange-coupled magnetic nanoparticles for efficient heat induction. Nat Nanotech 2011;6:418–22.
[3] Laurent S, Mahmoudi M. Superparamagnetic iron oxide nanoparticles: promises for diagnosis and treatment of cancer. Int J Mol Epidemiol Genet 2011;2:367–90.
[4] Yang HW, Hau MY, Liu HL, Huang CY, Tsai RY, Lu YJ, et al. Self-protecting core–shell magnetic nanoparticles for targeted, traceable, long half-life delivery of BCNU to gliomas. Biomaterials 2011;32:6523–32.
[5] Maier-Hauff K, Ulrich F, Nestler D, Niehoff H, Wust P, Thiesen B, et al. Efficacy and safety of intratumoral thermotherapy using magnetic iron-oxide nanoparticles combined with external beam radiotherapy on patients with recurrent glioblastoma multiforme. J Neurooncol 2011;103:317–24.
[6] Maier-Hauff K, Rothe R, Scholz R, Gneveckow U, Wust P, Thiesen B, et al. Intracranial thermotherapy using magnetic nanoparticles combined with external beam radiotherapy: results of a feasibility study on patients with glioblastoma multiforme. J Neurooncol 2007;81:53–60.
[7] Johannsen M, Gneveckow U, Thiesen B, Taymoorian K, Cho CH, Waldöfner N, et al. Thermotherapy of prostate cancer using magnetic nanoparticles: feasibility, imaging, and three-dimensional temperature distribution. Eur Urol 2007;52:1653–61.
[8] Johannsen M, Gneveckow U, Taymoorian K, Thiesen B, Waldöfner N, Scholz R, et al. Morbidity and quality of life during thermotherapy using magnetic nanoparticles in locally recurrent prostate cancer: results of a prospective phase I trial. Int J Hyperthermia 2007;23:315–23.
[9] Moroz P, Jones SK, Gray BN. Status of hyperthermia in the treatment of advanced liver cancer. J Surg Oncol 2001;77:259–69.
[10] Rosensweig RE. Heating magnetic fluid with alternating magnetic field. J Magn Magn Mater 2002;252:370–4.
[11] Yu TJ, Li PH, Tseng TW, Chen YC. Multifunctional Fe_3O_4/alumina core/shell MNPs as photothermal agents for targeted hyperthermia of nosocomial and antibiotic-resistant bacteria. Nanomedicine 2011;6:1353–63.
[12] Liao MY, Lai PS, Yu HP, Lin HP, Huang CC. Innovative ligand-assisted synthesis of NIR-activated iron oxide for cancer theranostics. Chem Commun 2012;48:5319–21.
[13] Li L, Xie J, Zhang X, Chen J, Luo Y, Zhang L, et al. Retrospective study of photodynamic therapy vs photodynamic therapy combined with chemotherapy and chemotherapy alone on advanced esophageal cancer. Photodiag Photodyn Ther 2010;7:139–43.
[14] Gray J, Fullarton G. The current role of photodynamic therapy in oesophageal dysplasia and cancer. Photodiag Photodyn Ther 2007;4:151–9.
[15] Eichler J, Liebetruth J, London RA, Ziegenhagen L. Temperature distribution for combined laser hyperthermia–photodynamic therapy in the esophagus. Med Eng Phys 2000;22:307–12.
[16] Muijs CT, Beukema JC, Pruim J, Mul VE, Groen H, Plukker JT, et al. A systematic review on the role of FDG-PET/CT in tumour delineation and radiotherapy planning in patients with esophageal cancer. Radiother Oncol 2010;97:165–71.
[17] van Vilsteren FG, Bergman JJ. Endoscopic therapy using radiofrequency ablation for esophageal dysplasia and carcinoma in Barrett's esophagus. Gastrointest Endosc Clin N Am 2010;20:55–74.
[18] Bumb A, Brechbiel MW, Choyke PL, Fugger L, Eggeman A, Prabhakaran D, et al. Synthesis and characterization of ultra-small superparamagnetic iron oxide nanoparticles thinly coated with silica. Nanotechnology 2008;19:335601 (6pp).
[19] Park J, An K, Hwang Y, Park JG, Noh HJ, Kim JY, et al. Ultra-large-scale syntheses of monodisperse nanocrystals. Nat Mater 2004;3:891–5.
[20] Andrés Vergés M, Costo R, Roca AG, Marco JF, Goya GF, Serna CJ, et al. Uniform and water stable magnetite nanoparticles with diameters around the monodomain–multidomain limit. J Phys D Appl Phys 2008;41:134003 (10pp).
[21] Liu X, Tao H, Yang K, Zhang S, Lee ST, Liu Z. Optimization of surface chemistry on single-walled carbon nanotubes for in vivo photothermal ablation of tumors. Biomaterials 2011;32:144–51.
[22] Yang K, Zhang S, Zhang G, Sun X, Lee ST, Liu Z. Graphene in mice: ultrahigh in vivo tumor uptake and efficient photothermal therapy. Nano Lett 2010;10:3318–23.
[23] Chu M, Peng J, Zhao J, Liang S, Shao Y, Wu Q. Laser light triggered-activated carbon nanosystem for cancer therapy. Biomaterials 2013;34:1820–32.
[24] Hirsch LR, Stafford RJ, Bankson JA, Sershen SR, Rivera B, Price RE, et al. Nanoshell-mediated near-infrared thermal therapy of tumors under magnetic resonance guidance. Proc Natl Acad Sci U S A 2003;100:13549–54.
[25] Chu M, Pan X, Zhang D, Wu Q, Peng J, Hai W. The therapeutic efficacy of CdTe and CdSe quantum dots for photothermal cancer therapy. Biomaterials 2012;33:7071–83.
[26] Thorek DL, Chen AK, Czupryna J, Tsourkas A. Superparamagnetic iron oxide nanoparticle probes for molecular imaging. Ann Biomed Eng 2006;34:23–38.